



LUND UNIVERSITY

Secondary bonding interactions in biomimetic [2Fe-2S] clusters

Ballmann, Joachim; Dechert, Sebastian; Bill, Eckhard; Ryde, Ulf; Meyer, Franc

Published in:
Inorganic Chemistry

DOI:
[10.1021/ic702095a](https://doi.org/10.1021/ic702095a)

2008

Document Version:
Peer reviewed version (aka post-print)

[Link to publication](#)

Citation for published version (APA):
Ballmann, J., Dechert, S., Bill, E., Ryde, U., & Meyer, F. (2008). Secondary bonding interactions in biomimetic [2Fe-2S] clusters. *Inorganic Chemistry*, 47(5), 1586-1596. <https://doi.org/10.1021/ic702095a>

Total number of authors:
5

Creative Commons License:
Unspecified

General rights

Unless other specific re-use rights are stated the following general rights apply:
Copyright and moral rights for the publications made accessible in the public portal are retained by the authors and/or other copyright owners and it is a condition of accessing publications that users recognise and abide by the legal requirements associated with these rights.

- Users may download and print one copy of any publication from the public portal for the purpose of private study or research.
- You may not further distribute the material or use it for any profit-making activity or commercial gain
- You may freely distribute the URL identifying the publication in the public portal

Read more about Creative commons licenses: <https://creativecommons.org/licenses/>

Take down policy

If you believe that this document breaches copyright please contact us providing details, and we will remove access to the work immediately and investigate your claim.

LUND UNIVERSITY

PO Box 117
221 00 Lund
+46 46-222 00 00

Secondary bonding interactions in biomimetic [2Fe2S] clusters

Joachim Ballmann,[†] Sebastian Dechert,[†] Eckhard Bill,[‡] Ulf Ryde,^{*,§} Franc Meyer,^{*,†}

Institut für Anorganische Chemie, Georg-August-Universität, Tammannstrasse 4, D-37077
Göttingen, Germany.

Max-Planck-Institut für Bioanorganische Chemie, Stiftstrasse 34-36, D-45470 Mülheim an der
Ruhr, Germany

Department of Theoretical Chemistry, Lund University, Chemical Centre, S-22100 Lund,
Sweden

Received (to be filled by editorial staff)

* To whom correspondence should be addressed. E-mail address: franc.meyer@chemie.uni-goettingen.de (F. M.); Ulf.Ryde@toekem.lu.se (U. R.). Phone: +49-551-39-3012 (F. M.); +46-46-222-4502 (U. R.). Fax: +49-551-39-3063 (F. M.); +46-46-222-4543 (U. R.).

[†] Georg-August-Universität

[‡] Max-Planck-Institut für Bioanorganische Chemie

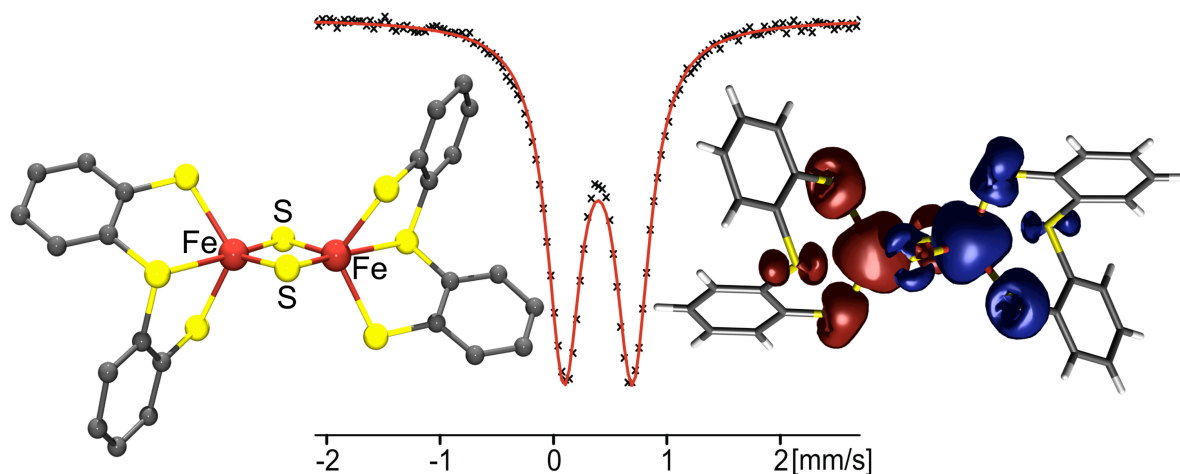
[§] Lund University

1

Abstract

A series of synthetic [2Fe2S] complexes with terminal thiophenolate ligands and tethered ether or thioether moieties has been prepared and investigated in order to provide models for the interaction of additional donor atoms with the Fe atoms in biological [2Fe2S] clusters. X-ray crystal structures have been determined for six new complexes that feature appended Et (**1^C**), OMe (**1^O**), or SMe (**1^S**) groups, or with a methylene group (**2^C**), an ether-O (**2^O**), or an thioether-S (**2^S**) linking two aryl groups. The latter two systems provide a constrained chelate arrangement that induces secondary bonding interactions with the ether-O and thioether-S, which is confirmed by DFT calculations that also reveal significant spin density on those fifth donor atoms. Structural consequences of the secondary bonding interactions are analyzed in detail, and effects on the spectroscopic and electronic properties are probed by UV-Vis, Mössbauer, and ¹H NMR spectroscopy, as well by SQUID measurements and cyclic voltammetry. The potential relevance of the findings for biological [2Fe2S] sites is considered.

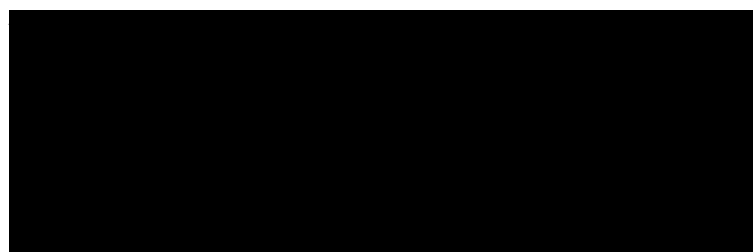
Graphical Contents Entry



Keywords: Bioinorganic Chemistry, Iron-sulfur clusters, S-ligands, Mössbauer spectroscopy, DFT calculations.

Introduction

Iron-sulfur clusters are among the most versatile cofactors in nature, involved in a broad range of biological processes.¹ The understanding of their primary function as electron transfer sites has benefited significantly from the investigation of synthetic analogues, which appeared on the scene in the early 1970s.² During the last few years, interesting new functions of iron-sulfur clusters in, *inter alia*, radical generation, substrate binding and catalysis, gene-regulation and sensing of iron and oxygen were discovered and explored.^{3,4} As a prominent example, the enzyme biotin synthase, containing both [4Fe4S] and [2Fe2S] sites, mediates the insertion of sulfur into dethiobiotin in a SAM-based radical process.⁵ One of the bridging sulfides of the [2Fe2S] core is postulated to be the source of the sulfur that is transferred during the final step of the biosynthesis of this essential vitamin. A recent crystallographic analysis of biotin synthase revealed a unique coordination environment of the [2Fe2S] cluster, with three terminal cysteine-S ligands and an unprecedented terminal arginine-N that causes a noticeable distortion of the local cluster symmetry (Scheme 1).⁶ While the arginine residue does not seem to be essential for the catalytic reaction of biotin synthase,⁷ the biological relevance of this very unusual cluster coordination remains to be elucidated. One should note that arginine is a very rare ligand in metalloproteins,⁸ although guanidine-metal interactions are quite flexible and may comprise syn, anti and chelating coordination.



Scheme 1

In another new turn in biological [2Fe2S] cluster chemistry, considerable conformational differences have recently been reported for a [2Fe2S] ferredoxin from *Rhodobacter capsulatus* in its oxidized and reduced forms.⁹ Upon reduction the [2Fe2S] core switches from a planar to a

distorted lozenge geometry, and the movement of a methionine side chain results in the methionine-S δ atom approaching a bridging sulfide of the cluster at less than 2.9 Å (Scheme 1). The functional significance of these changes are still unclear, but it has been speculated that the proximity of the electron-rich thioether-S may contribute to controlling the redox potential of the cluster by modulating the overall electrostatic environment.

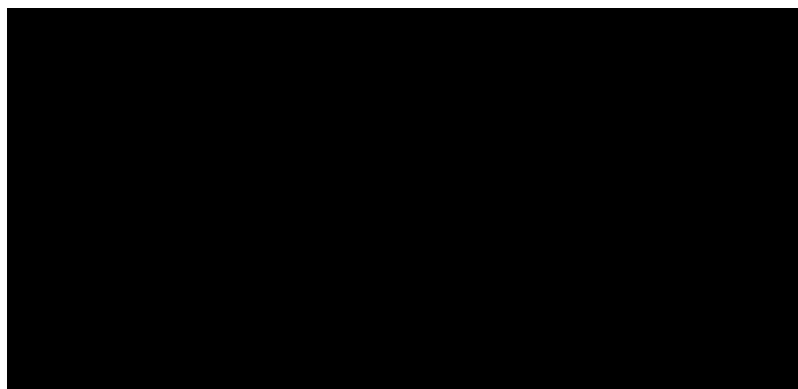
In the context of those new developments in iron-sulfur cluster chemistry, we realized that geometric distortions and consequences of secondary bonding interactions have only been scarcely addressed for synthetic [2Fe2S] complexes.¹⁰ Holm and coworkers had previously studied the occurrence of secondary bonding interactions in [4Fe4S] clusters, where the terminal thiolate ligands contained potentially coordinating *ortho*-substituents, [Fe₄S₄(SC₆H₄-*o*-X)₄]²⁻ with X = OH, OMe, NH₂.¹¹ Indeed, unique Fe-site chemistry during catalytic turnover has recently been demonstrated for the [4Fe4S] cluster in ferredoxin:thioredoxin reductase (FTR), which involves interaction of a disulfide with one Fe, followed by breaking of the disulfide bond and five-coordination of that unique Fe site with two cysteinate ligands.¹² In order to assess whether such interactions are feasible in [2Fe2S] systems and to evaluate possible effects on spectroscopic and electronic properties of the cluster, we have now examined a series of synthetic [2Fe2S] clusters coordinated by thiophenolate derivatives bearing additional donor sites. Some particularly preorganized chelate ligands have been employed to enforce additional bonding interactions, and DFT calculations have been carried out to corroborate the structural and spectroscopic findings.

4

Results and Discussion

Synthesis and structural characterization. A series of new [2Fe2S] clusters with terminal thiophenolate derivatives bearing substituents in the *ortho* position of the phenyl ring have been synthesized by means of standard salt metathesis reactions starting from the readily available (NEt₄)₂[Fe₂S₂Cl₄], Scheme 2. Complexes **1^C**, **1^O** and **1^S** were obtained in moderate to good yields, and crystalline material could be obtained by diffusion of diethylether into DMF solutions

(**1^O**, **1^S**) or by slowly cooling a saturated MeCN solution from room temperature to -20°C (**1^C**). The ether or thioether substituents in **1^O** and **1^S**, respectively, were anticipated to potentially interact with the Fe centers, and the alkyl substituted **1^C** was prepared to allow accurate structural comparison with an analogous system that lacks the additional donor groups.



Scheme 2: Synthesis of complexes **1^C**, **1^O**, and **1^S**.

Molecular structures of **1^C**, **1^O**, and **1^S** are quite similar, and the anion of **1^S** is shown in Figure 1 as an example (for molecular structures of **1^C** and **1^O** see Figures S1 and S2). Selected structural parameters are listed in Table 1, other interatomic distances and angles are given in the supplementary information (Table S1). In all cases, the tetraethylammonium cations are well separated from the [2Fe2S] dianions. Compound **1^O** crystallizes in the monoclinic space group $P2_1/c$ with four formula units per unit cell. The asymmetric unit contains two crystallographically independent anion-fragments, and each [2Fe2S] dianion consists of two fragments as a centrosymmetric dimer with crystallographically imposed C_i symmetry. **1^S** crystallizes in the monoclinic space group $P2_1/n$ with two molecules per unit cell and also features crystallographically imposed C_i symmetry. The cores of both **1^O** and **1^S** are close to effective C_{2h} symmetry due to the only marginal differences between the Fe1-S2 and Fe1-S3 bond lengths. The alkyl derivate **1^C** crystallizes in the monoclinic space group $C2/c$ with four formula units and eight acetonitrile molecules per unit cell. In contrast to **1^O** and **1^S**, the anions of **1^C** are perfectly C_2 -symmetric monomers, with the C_2 -axis along Fe1 and Fe2. Bond lengths

Fe1-S1 and Fe1-S6 and all bond lengths between the iron atoms and the terminal thiophenolate sulfur atoms are almost identical for **1^C**, but in this case differences in the angles S2-Fe1-S3 and S4-Fe2-S5 cause deviations from an effective C_{2h} -symmetry. The Fe \cdots Fe distances of **1^O**, **1^S**, and **1^C** resemble those of the other $[\text{Fe}_2\text{S}_2(\text{SR})_4]^{2-}$ clusters with terminal thiophenolate derivatives that have been characterized to date (around 2.67 – 2.70 Å). All type **1** complexes contain symmetric $(\text{Fe}_2\text{S}_2)^{2+}$ cores with a perfectly planar structure (dihedral angles Fe1-S1-Fe2-S6 = 0°). Distances Fe-^LS and Fe-^μS as well as angles ^LS-Fe-^LS and ^μS-Fe-^μS are in the usual range (Table 1).

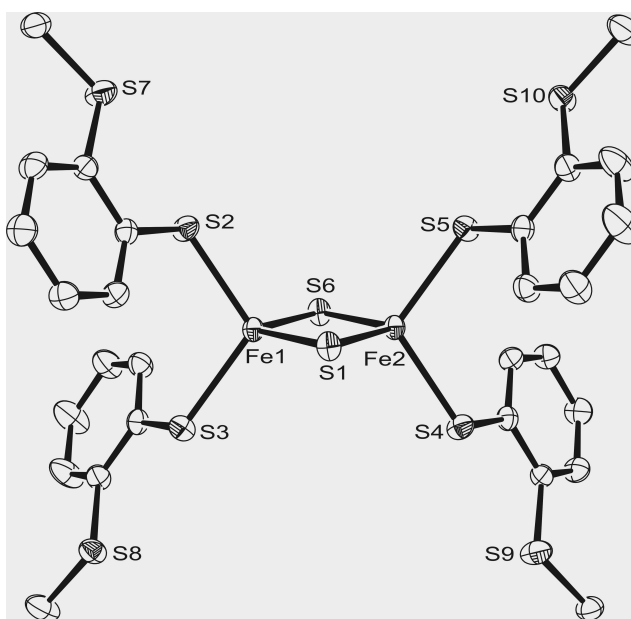


Figure 1: ORTEP plot (50% probability thermal ellipsoids) of the molecular structure of the anion of **1^S**. All hydrogen atoms have been omitted for clarity.

6

¹) Beinert, H.; Holm, R. H.; Münck, E. *Science* **1997**, *277*, 653-659.

²) Rao, P.V.; Holm, R.H. *Chem. Rev.* **2004**, *104*, 527-560.

³) Fontecave, M. *Nature Chemical Biology* **2006**, *2*, 171-174.

⁴) Beinert, H. *J. Biol. Inorg. Chem.* **2000**, *5*, 2-15.

⁵) Jarrett, J.T. *Arch. Biochem. Biophys.* **2005**, *433*, 312-321.

⁶) Berkovitch, F.; Nicolet, Y.; Wan, J. T.; Jarret, J. T.; Drennan, C. L. *Science* **2004**, *303*, 76-79.

⁷) Broach, R.B.; Jarrett, J.T. *Biochem.* **2006**, *45*, 14166-14174.

⁸) Di Costanzo, L.; Flores Jr., L.V.; Christianson, D.W. *Proteins* **2006**, *65*, 637-642.

⁹() Sainz, G.; Jakoncic, J.; Sieker, L.C.; Stojanoff, V.; Sanishvili, N.; Asso, M.; Bertrand, P.; Armengaud, J.; Jouanneau, Y. *J. Biol. Inorg. Chem.* **2006**, *11*, 235-246.

¹⁰() The effect of NH \cdots S hydrogen bonds in synthetic [2Fe2S] clusters has been studied: Ueyama, N.; Yamada, Y.; Okamura, T.; Kimura, S.; Nakamura, A. *Inorg. Chem.* **1996**, *35*, 6473-6484.

¹¹() Johnson, R.E.; Papaefthymiou, G.C.; Frankel, R.B.; Holm, R.H. *J. Am. Chem. Soc.* **1983**, *105*, 7280-7287.

¹²() Jameson, G.N.L.; Walters, E.M.; Manieri, W.; Schürmann, P.; Johnson, M.K.; Huynh, B.H. *J. Am. Chem. Soc.* **2003**, *125*, 1146-1147.

Table 1: Selected structural parameters for $(\text{NEt}_4)_2[\text{Fe}_2\text{S}_2(\text{SR})_4]$ clusters (SR = thiophenolate derivative). Selected interatomic distances are given in [Å] and angles in [°].

complex	Fe \cdots Fe	Fe- $^{\mu}\text{S}$	Fe- $^{\text{L}}\text{S}$	Fe- $^{\mu}\text{S}$ -Fe	$^{\mu}\text{S}$ -Fe- $^{\mu}\text{S}$	$^{\text{L}}\text{S}$ -Fe- $^{\text{L}}\text{S}$	
$(\text{NEt}_4)_2[\text{Fe}_2\text{S}_2(\text{SC}_6\text{H}_5)_4]^{\text{a},13}$	2.691(2)	2.197(3) 2.197(3)	2.296(3) 2.306(3)	75.5(2)	104.5(2)	110.0(2)	0.9
$(\text{NEt}_4)_2[\text{Fe}_2\text{S}_2(\text{SC}_6\text{H}_4\text{Me-4})_4]^{\text{a},14}$	2.691(1)	2.200(1) 2.202(1)	2.312(1) 2.312(1)	75.39(4)	104.61(4)	111.20(4)	0.9
$(\text{NEt}_4)_2[\text{Fe}_2\text{S}_2(\text{SC}_6\text{H}_4\text{Cl-4})_4]^{\text{a},15}$	2.703(2)	2.196(3) 2.198(3)	2.296(3) 2.309(3)	75.92(9)	104.08(9)	100.3(2)	0.9
$(\text{NEt}_4)_2[\text{Fe}_2\text{S}_2(\text{SC}_6\text{H}_2\text{Me}_3\text{-2,4,6})_4]^{\text{a},16}$	2.698(5)	2.195(6) 2.204(6)	2.299(8) 2.318(6)	75.62(20)	104.4(3)	107.9(3)	0.9
$(\text{NEt}_4)_2[\text{Fe}_2\text{S}_2(\text{SC}_6\text{H}_3(\text{tBuCONH})_2\text{-2,6})_4]^{\text{b},10}$	2.671(6)	2.198(7) 2.203(6)	2.308(8) 2.328(7)	74.8(2)	104.1(2)	107.7(3)	0.9
1^C ^{a,e}	2.683(2)	2.191(2) 2.198(2)	2.304(2) 2.306(3)	75.38(6)	104.38(9) 104.87(9)	112.2(2) 116.2(2)	0.9 0.9
1^O ^{a,f}	2.6992(6) 2.7041(5)	2.2049(6) 2.2028(6) 2.2112(6) 2.2033(6)	2.3015(6) 2.3081(6) 2.3030(6) 2.3192(6)	75.55(2) 75.53(2)	104.47(2) 104.45(2)	111.18(2) 112.21(2)	0.9 0.9
1^S ^a	2.6908(4)	2.1931(4) 2.1933(4)	2.3048(4) 2.3239(5)	75.68(2)	104.32(1)	110.66(2)	0.9
2^C ^a	2.6918(4)	2.1977(5) 2.2010(5)	2.2933(5) 2.3392(5)	75.46(2)	104.54(2)	109.82(2)	0.9
2^O ^{c,e}	2.7381(3)	2.2064(5) 2.2028(5) 2.2050(5) 2.2147(5)	2.3309(5) 2.3425(5) 2.3258(5) 2.3421(5)	76.73(2) 76.61(2)	103.15(1) 103.50(2)	110.22(2) 116.71(2)	0.9 0.9
2^S ^{d,e}	2.802(2)	2.212(4) 2.221(4) 2.237(3) 2.209(4)	2.324(3) 2.358(3) 2.369(3) 2.341(3)	78.06(12) 78.45(12)	101.9(2) 101.5(2)	113.1(2) 115.8(2)	0.9 0.9

(a) perfectly planar Fe_2S_2 core with dihedral angle $\text{Fe}-^{\mu}\text{S}-\text{Fe}-^{\mu}\text{S} = 0^\circ$. (b) $\text{Fe}-^{\mu}\text{S}-\text{Fe}-^{\mu}\text{S} = 4.20^\circ$. (c) $\text{Fe}-^{\mu}\text{S}-\text{Fe}-^{\mu}\text{S} = 0.71^\circ$. (d) $\text{Fe}-^{\mu}\text{S}-\text{Fe}-^{\mu}\text{S} = 2.61^\circ$. (e) iron atoms are crystallographically independent. (f) two crystallographically independent molecules.

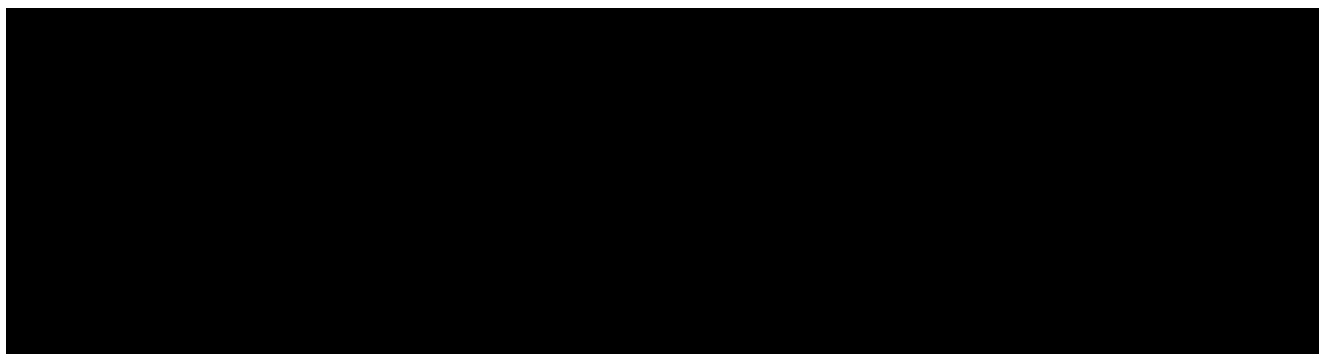
¹³) Jinhua, C.; Changneng, C. *Jiegou Huaxue (J. Struct. Chem.)* **1985**, 4, 199-202.

¹⁴) Mayerle, J. J.; Denmark, S. E.; DePamphilis, B. V.; Ibers, J. A.; Holm, R. H. *J. Am. Chem. Soc.* **1975**, 97, 103

¹⁵) Jinhua, C.; Changneng, C. *Jiegou Huaxue (J. Struct. Chem.)* **1988**, 7, 43-46.

¹⁶) Ueyama, N.; Ueno, S.; Sugawara, T.; Tatsumi, K.; Nakamura, A.; Yasuoka, N. *J. Chem. Soc., Dalton Trans.* **1**

It is obvious from the X-ray structural analyses of **1^O** and **1^S** that no interaction between the Fe atoms and the ether or thioether groups occurs in the solid state, and both molecules adopt conformations very similar to that found for the alkyl analogue **1^C**. The substituents do not induce any significant structural distortion, as evaluated by the τ_4 -values (Table 1).¹⁷ In order to enforce secondary interactions with the ether or thioether moiety in a more rigid chelate situation, the related systems **2^C**, **2^O**, and **2^S** were synthesized starting from the tethered bis(benzenethiolato) ligands (Scheme 3). Here the yield decreased in the order **2^C** > **2^O** > **2^S** due to the formation of significant amounts of undesired mononuclear complexes such as **3^S**. It should be noted that type **3** complexes become the preferred products with increasing donor strength of the potentially tridentate ligands, and no type **2** [2Fe2S] cluster could be isolated for the related systems with N- or P-based linkers (X = NMe, PPh).¹⁸



Scheme 3: Synthesis of complexes **2^C**, **2^O**, and **2^S**.

Single crystals suitable for X-ray analysis were obtained by diffusion of diethyl ether into a saturated solution of the complex in MeCN (for **2^C**) or by slow diffusion of diethyl ether into DMF solutions (for **2^O** and **2^S**). Molecular structures of the anions of **2^C**, **2^O** and **2^S** are depicted in Figure 2, and selected structural parameters are included in Table 1 (other interatomic distances and bond angles are given in Table S2 in the supporting information). **2^C** and **2^O** crystallize in the monoclinic space group $P2_1/c$ with two or four formula units per unit cell, respectively, while **2^S** crystallizes in $P2_1$ with two molecules per unit cell. In contrast to complexes **1^C**, **1^O**, **1^S**, and **2^C**, the asymmetric units of **2^O** and **2^S** each contain one complete

dianion and two well-separated tetraethylammonium cations. In both latter cases the point group symmetries of the clusters are reduced from apparent C_{2h} (with the horizontal mirror planes through Fe1, Fe2, S1, S2, X1 and X2 (X = ether-O or thioether-S atoms) and the perpendicular C_2 axes through the centroids of the Fe_2S_2 -cores). Bond lengths Fe-L-S and Fe- μ S are not drastically different from those of other [2Fe2S] clusters coordinated by thiophenolate derivatives (summarized in Table 1), but a slight bond elongation is discernible for 2^S . Differences are more significant for the Fe \cdots Fe separations and the angles μ S-Fe- μ S. While the elongation of the Fe \cdots Fe distance by approximately 4 pm is still moderate in 2^O (2.738(1) Å versus 2.683 – 2.704 Å for type **1** complexes and 2^C), it is much more pronounced for 2^S (2.802(2) Å). This goes along with a decrease in the μ S-Fe- μ S angles and a corresponding increase of the Fe- μ S-Fe angles, as well as some distortion of the $(Fe_2S_2)^{2+}$ cores away from planarity (dihedral angles Fe1-S1-Fe2-S2 are 0.71° for 2^O and 2.61° for 2^S). It is interesting to note that [2Fe2S] clusters in proteins also tend to have longer Fe \cdots Fe than typical synthetic $[Fe_2S_2(SR_4)]^{2-}$ complexes such as the above type **1** systems, e.g., $d(Fe\cdots Fe) = 2.733(7)$ Å in the oxidized form of a green algae ferredoxin.¹⁹

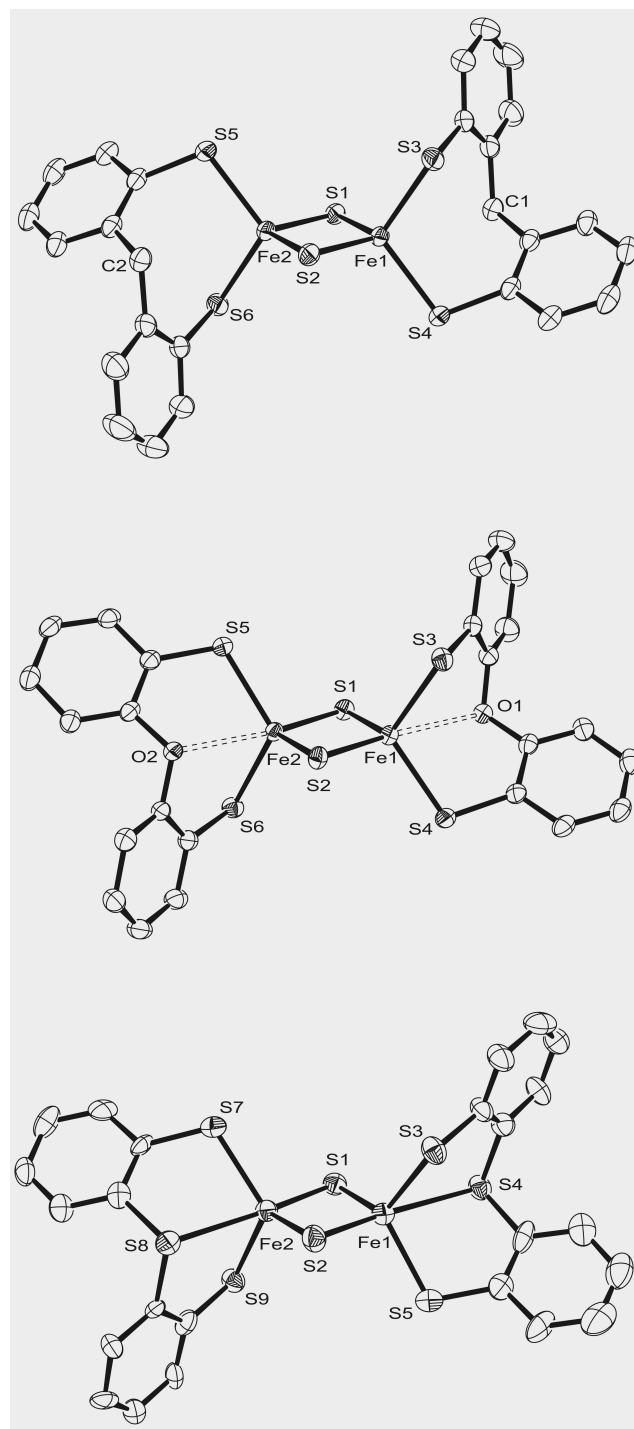


Figure 2: ORTEP plots (50% probability thermal ellipsoids) of the molecular structures of the dianions of 2^C (top), 2^O (middle), and 2^S (bottom). All hydrogen atoms have been omitted for clarity.

Inspection of the τ_4 values reveals an increasing deviation from tetrahedral geometry for the $\{\text{FeS}_4\}$ in the order 2^C ($\tau_4 = 0.960$) < 2^O ($\tau_4 = 0.914/0.892$) < 2^S ($\tau_4 = 0.876/0.866$), signifying involvement of the additional ether or thioether donor in metal coordination and a gradual

transition to trigonal bipyramidal iron environment within this series of complexes. For 2^S a τ_4 value close to the theoretical value of 0.85 for an ideal trigonal bipyramid is observed, with the additional donor site in an axial position. The distances $Fe\cdots X$ ($X = CH_2, O, S$) decrease in the order 2^C [$d(Fe\cdots C) = 3.335(2)$] > 2^O [$d(Fe\cdots O) = 2.813(2)/2.679(2)$] \approx 2^S [$d(Fe\cdots S) = 2.914(4)/2.777(4)$], which is accompanied by decreasing distances between the iron atoms and the equatorial planes (which for 2^S are given by S1/S3/S5 and S2/S7/S9) in the series 2^C [0.6798(2) Å] > 2^O [0.5811(2)/0.5110(2) Å] > 2^S (0.403(2)/0.375(2) Å]. The approach of the additional donor atoms in 2^O and 2^S causes a significant “out-of-plane distortion” compared to 2^C (**Figure 3**). This distortion can be quantified by comparing the angles between the planes through $^{Lig}S-Fe-^{Lig}S$ and the planes perpendicular to the Fe_2S_2 -diamond (constructed from the centroid of the Fe_2S_2 -core and the vector through the bridging sulfides as normal of the plane; see Figure 3). These angles increase in the row 2^C (3.51(1)°) < 2^O (13.52(3)°) < 2^S (23.79(11)°), whereas type **1** complexes are only slightly distorted (Figure S3).

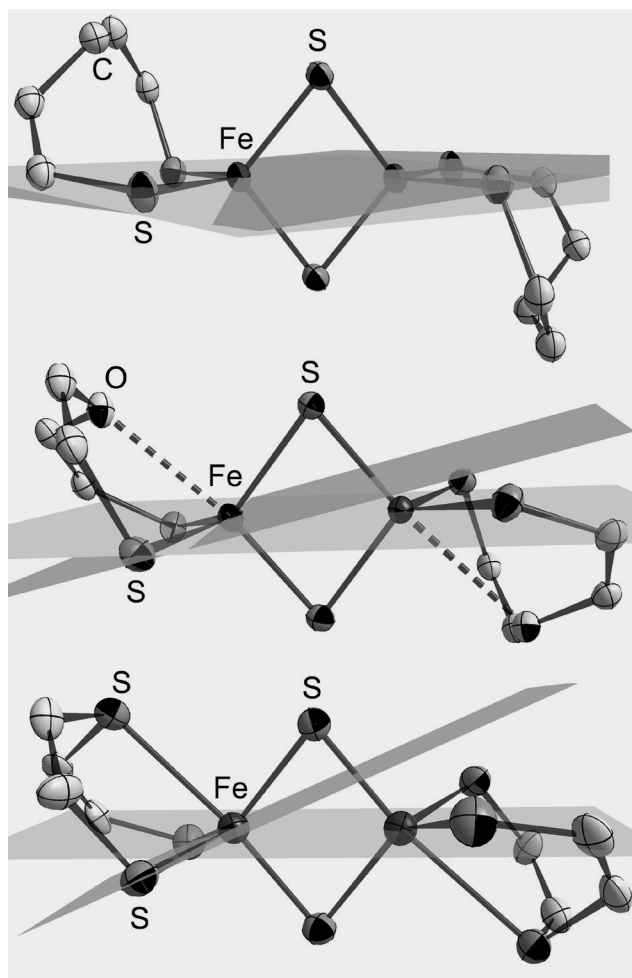


Figure 3: Illustration of increasing “out-of-plane distortion” in the order 2^C (top), S^O (middle) and 2^S (bottom). Counterions, protons and peripheral aromatic carbons are omitted for clarity.

Taken together, the structural features strongly suggest an increase in coordination number for the Fe atoms and significant structural distortion of the $[\text{Fe}_2\text{S}_2(\text{SR})_4]^{2-}$ cores in 2^O and 2^S due to secondary bonding interactions with the ether-O or thioether-S atoms, respectively, in particular in the latter case. In order to probe the nature of these interactions and consequences for electronic structures of the $[2\text{Fe}_2\text{S}]$ clusters, detailed spectroscopic and DFT studies have been performed.

Spectroscopy and magnetic properties in the solid state. Zero-field Mössbauer spectra for all clusters have been recorded at 80 K. Spectral fits to the data were obtained by using Lorentzian line doublets with isomer shifts δ and quadrupole splittings ΔE_Q summarized in

Table 2. It should be noted that Mössbauer data for synthetic [2Fe2S] compounds with purely thiolato terminal ligation are still quite scarce.²

¹⁷() The τ_4 value has been proposed as a simple geometry index to quantify the distortion from tetrahedral geometry ($\tau_4 = 1$) for four-coordinate species and is calculated by $\tau_4 = 1/141^\circ \times (360^\circ - \alpha - \beta)$, with α and β defined as the two largest angles (Ligand)-(Metal)-(Ligand) in the four coordinate complex: Yang, L.; Powell, D. R.; Houser, R. P. *Dalton Trans.* **2007**, 955-964.

¹⁸() Ballmann, J.; Dechert, S.; Meyer, F. unpublished results.

¹⁹() Bes, M. T.; Parisini, E.; Inda, L.A.; Saraiva, L.M.; Peleato, M.L.; Sheldrick, G.M. *Structure* **1999**, 7, 1201-1211.

Table 2: Spectroscopic, magnetic and electrochemical data for the new complexes.

complex	δ (ΔE_Q) [mm/s] ^a	λ_{\max} [nm] (ϵ [$M^{-1}cm^{-1}$]) ^b	J [cm^{-1}] ^c	E_p [V] ^d
(NEt ₄) ₂ [Fe ₂ S ₂ (SPh) ₄] 14	0.28 (0.32)	333 (19500), 490 (11200)	not reported	-1.11 ^e
(NEt ₄) ₂ [Fe ₂ S ₂ (S ₂ - <i>o</i> -xyl) ₂] 14 ^f Error! Bookmark not defined.	0.28 (0.36)	294 (14500), 338 (16200), 414 (11000), ~ 455 (9200, <i>sh</i>), 590 (4800)	-149±8	-1.51 ^f
1^C	0.30 (0.44)	331 (29000), 476 (15000)	-197	-1.24
1^O	0.29 (0.42)	296 (58000, <i>sh</i>), 336 (33000), 509 (15000)	-180	-1.32
1^S	0.29 (0.44)	307 (50000), 350 (27000, <i>sh</i>), 491 (12000)	-181	-1.14
2^C	0.30 (0.56)	291 (16000), 352 (20500), 444(10000), 547 (10500), 616 (6500)	-204	-1.24
2^O	0.32 (0.56)	329 (19000), 486 (9000)	-158	-1.48
2^S	0.39 (0.61)	288 (59000), 322 (37000, <i>sh</i>), 475 (11000)	-126	-0.99

(a) ⁵⁷Fe Mössbauer parameters at 80 K, relative to Fe metal at room temperature. (b) recorded in DMF solution at room temperature. (c) values obtained from simulation of SQUID data (see text). (d) cathodic peak potentials in DMF/0.1 M [NBu₄]PF₆ at a scan rate of 100 mV/s; values vs. the Cp*₂Fe/Cp*₂Fe⁺ couple. (e) Half-wave potential $E_{1/2}$ of the reversible process in DMF vs. SCE is -1.09 V,14 corresponding to -1.11 V vs. the Cp*₂Fe/Cp*₂Fe⁺ couple. (f) Half-wave potential $E_{1/2}$ in DMF vs. SCE is -1.49 V,14 corresponding to -1.51 V vs. the Cp*₂Fe/Cp*₂Fe⁺ couple.

Mössbauer spectra of **1^S** and **2^S** are representative examples for type **1** and type **2** cluster compounds and are depicted in Figure 3 (spectra for **1^C**, **1^O**, **2^C** and **2^O** are provided in the supplementary information, Figures S4 – S7). All six compounds exhibit isomer shifts δ in the range 0.29 – 0.39 mm/s, which is typical for high-spin ferric ions. Whereas δ parameters for type **1** systems and **2^C** are comparable to those of parent $[\text{Fe}_2\text{S}_2(\text{SPh})_4]^{2-}$ and the related $[\text{Fe}_2\text{S}_2(\text{S}_2\text{-o-oxyl})_2]^{2-}$, values for type **2** complexes are clearly increasing in the order **2^C** < **2^O** < **2^S**. Isomer shifts have been empirically related to the oxidation state s of the iron atoms according to $\delta = 1.43 - 0.40s$ (correlation found for tetrahedral $\{\text{FeS}_4\}$ sites at 77 K by linear regression analysis).²⁰ Applying this equation to **1^C**, **1^O**, **1^S** and **2^C** reveals formal oxidation states s between 2.825 and 2.850, since the coordinated electron-donating thiophenolates increase the electron densities at the iron sites. Significantly lower values are found for **2^O** ($s = 2.78$) and **2^S** ($s = 2.60$), however, suggesting that additional interactions between the ether-O or thioether-S and the iron atoms are present, thus further increasing the electron densities at the ferric ions. Hence the above equation seems to be invalid for **2^O** and **2^S**, due to the presence of $\{\text{FeS}_4\text{O}\}$ or $\{\text{FeS}_5\}$ motives rather than tetrahedral $\{\text{FeS}_4\}$.

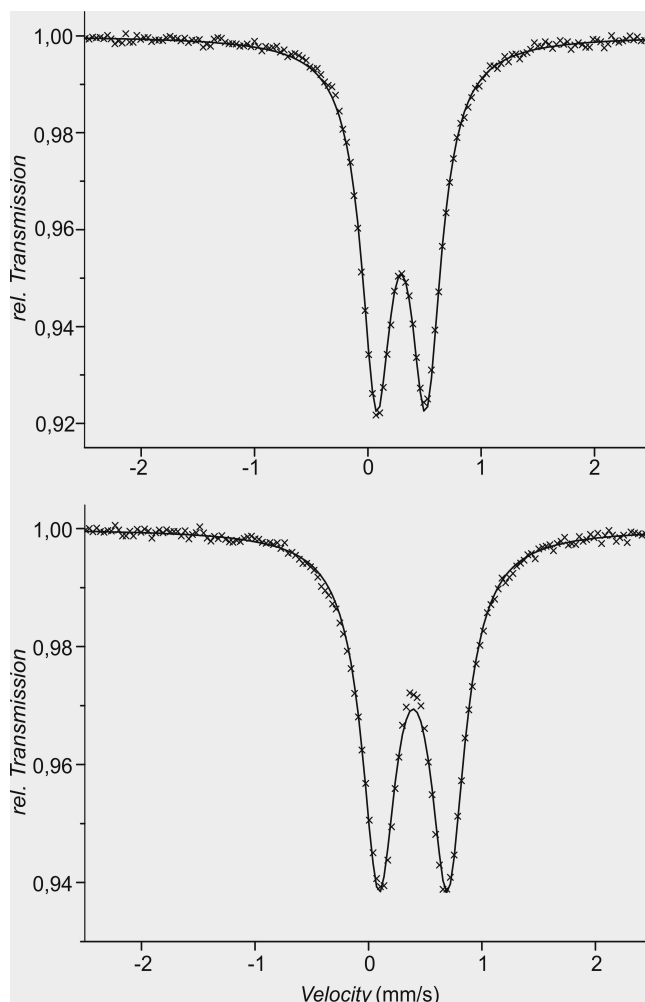


Figure 3: Zero-field Mössbauer spectra of 1^S (top) and 2^S (bottom) at 80 K. The solid lines are Lorentzian doublets fitted to the experimental values (crosses).

Quadrupole splittings ΔE_Q are similar in the series 1^C (0.44 mm/s), 1^O (0.42 mm/s), and 1^S (0.44 mm/s) and in the series 2^C (0.56 mm/s), 2^O (0.56 mm/s) and 2^S (0.61 mm/s). Values for type **1** complexes are comparable to those reported previously for synthetic S-coordinated [2Fe2S] clusters ($[\text{Fe}_2\text{S}_2(\text{S}_2\text{-}o\text{-xyl})_2]^{2-}$: $\delta = 0.28$ mm/s, $\Delta E_Q = 0.36$ mm/s; $[\text{Fe}_2\text{S}_2(\text{SPh})_4]^{2-}$: $\delta = 0.28$ mm/s, $\Delta E_Q = 0.32$ mm/s²¹), whereas quadrupole splittings for type **2** complexes are augmented by ≥ 0.2 mm/s compared to $[\text{Fe}_2\text{S}_2(\text{S}_2\text{-}o\text{-xyl})_2]^{2-}$ and $[\text{Fe}_2\text{S}_2(\text{SPh})_4]^{2-}$. It is interesting to note that oxidized ferredoxins exhibit quite large quadrupole splittings ΔE_Q in the range 0.6 mm/s – 0.8 mm/s,²² which is significantly larger than for previously synthesized [2Fe2S]

model systems but similar to ΔE_Q values of the distorted type **2** clusters (*spinach* Fd_{ox} : $\delta = 0.22$ mm/s, $\Delta E_Q = 0.65$ mm/s²¹; *Isca1*: $\delta = 0.27$ mm/s, $\Delta E_Q = 0.57$ mm/s²³).

Magnetic susceptibility measurements for all new complexes were carried out at 1 T from 2.0 to 290 K. Magnetic moments μ_{eff} at room temperature are in the range 1.7 – 2.6 μ_B , i.e., much lower than expected for two uncoupled ferric ($S = 5/2$) ions, and they rapidly decrease upon lowering the temperature (plots of μ_{eff} versus temperature for all cluster compounds are shown in Figures S8 – S13). This behavior is in accordance with significant antiferromagnetic coupling between the two ferric ions to give an $S = 0$ ground state, as is usually observed for [2Fe2S] clusters. Coupling constants J (**Table 2**) were determined by using a fitting procedure to the appropriate Heisenberg spin Hamiltonian for isotropic exchange coupling and Zeeman interaction: [REDACTED].²⁴ For type **1** complexes the coupling is very strong ($J \sim -180$ cm⁻¹) and is slightly higher than those observed for, e.g., dipyrromethane coordinated clusters (NEt₄)₂[R₂C(C₄H₃N)₂Fe(μ -S)₂Fe(NC₄H₃)₂CR₂] with terminal {N₂} ligation ($J \sim -170$ cm⁻¹).²⁵ Complex **2^C** exhibits the highest antiferromagnetic exchange constant $J = -204$ cm⁻¹ reported so far for synthetic [2Fe2S] clusters. The lower J value for compound **2^O** ($J = -158$ cm⁻¹) is comparable to that of (NBu₄)₂[Fe₂S₂(S₂-o-*xy*l)₂] ($J \sim -150$ cm⁻¹), whereas **2^S** ($J = -126$ cm⁻¹) exhibits the weakest antiferromagnetic coupling reported for synthetic [2Fe2S] clusters until now. It is likely that the decrease in antiferromagnetic coupling in the sequence **2^C** < **2^O** < **2^S** is caused by the widening of the Fe-^μS-Fe angles and the increasing Fe...Fe distance. A J value of -183 cm⁻¹ was reported for *spinach* Fd_{ox} .²⁶

Solution properties. All new complexes were characterized by NMR, cyclic voltammetry and UV-Vis spectroscopy in order to clarify whether the situation observed in the solid state is preserved in solution and whether secondary interactions are present or absent in polar solvents. Electronic absorption spectra in DMF solution are shown in Figure 5a for clusters **1^C**, **1^O** and **1^S**, and in Figure 5b for **2^C**, **2^O** and **2^S**. Spectral data are also compiled in **Table 2**.

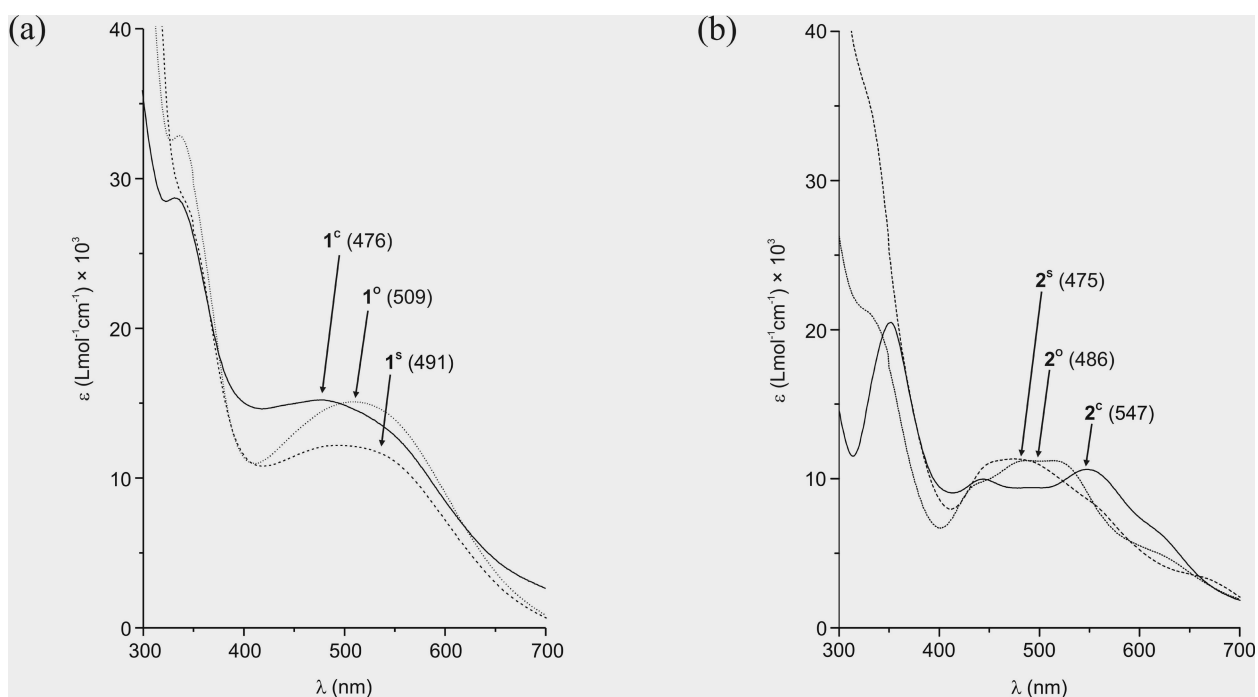


Figure 5: (a) Absorption spectra of $(\text{NEt}_4)_2[\text{Fe}_2\text{S}_2(\text{SC}_6\text{H}_4\text{-}o\text{-X})_4]$, X = CH_2Me (**1^c**), OMe (**1^o**), SMe (**1^s**) in DMF; (b) Absorption spectra of $(\text{NEt}_4)_2[\text{Fe}_2\text{S}_2(\text{SC}_6\text{H}_4\text{-X-C}_6\text{H}_4\text{S})_2]$, X = CH_2 (**2^c**), O (**2^o**), S (**2^s**) in DMF (wavelengths of visible band maxima are given in parentheses).

Compared to $(\text{NEt}_4)_2[\text{Fe}_2\text{S}_2(\text{SC}_6\text{H}_4\text{-}o\text{-Et})_4]$ (**1^c**), the π -electron donating methoxy (**1^o**) and thiomethyl substituents (**1^s**) are expected to lower the energies for the visible absorptions, which were assigned previously to thiophenolate-to-core charge transfer transitions.¹¹ Indeed a red-shift by 15 nm (**1^s**) or 33 nm (**1^o**) relative to **1^c** is observed. Any additional interaction of the ether or thioether functions with the iron atoms of the $[\text{2Fe2S}]$ core should decrease the substituent's electron donating ability towards the benzenethiolate but increase the electron density at the iron atoms, resulting in a blue shift of the ligand-to-metal charge transfer bands. Such trends have also been discussed for $[\text{4Fe4S}]$ clusters with substituted thiophenolate ligands and potential secondary bonding interactions.¹¹ Therefore the observed spectral shifts for **1^o** and **1^s** implicate that no chelate rings are formed in DMF solution, similar to the situation in the solid state. Consistent with these observations, the $^1\text{H-NMR}$ spectra of **1^o** and **1^s** in DMSO-d_6 show relatively sharp resonances for the methyl groups that are only slightly shifted with respect to the resonances for the free ligand, whereas secondary bonding interactions with the iron atoms

should significantly broaden these signals (spectra for 1^C , 1^O and 1^S are shown in Figures S14-S16). In contrast to type **1** complexes, a blue shift of the ligand-to-metal charge transfer bands is observed for 2^O and 2^S relative to 2^C . Since the trend in solution optical properties is in accordance with what is expected from the solid-state structures, it can be assumed that secondary bonding interactions are also present in solution for 2^O and 2^S .

The ^1H NMR spectrum for 2^O in deuterated DMSO is shown in Figure 6 as an example (spectra for 2^C and 2^S are given in Figures S17 and S18). Reasonably resolved spectra are obtained because of the strong antiferromagnetic coupling between the two ferric ions ($S = 0$ ground state), and all resonances appear as broad singlets. In addition to signals for the tetraethylammonium cations, isotropically shifted signals for the aromatic protons are observed.

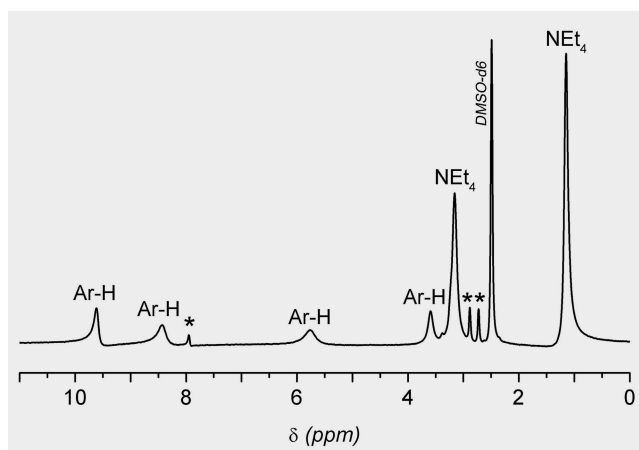


Figure 7: ^1H -NMR spectrum (500MHz, 25°C) of 2^O recorded in DMSO-d6 (residual DMF signals are marked by *).

Redox properties of all complexes have been examined by cyclic voltammetry in DMF/0.1 M $[\text{NBu}_4]\text{PF}_6$ at room temperature. The clusters 1^C , 1^O and 1^S all exhibit an irreversible reduction process with cathodic peak potentials around -1.2 V vs. the $\text{Cp}^*\text{Fe}/\text{Cp}^*\text{Fe}^+$ couple at scan rate 100 mV/s (**Table 2**, Figures S19 – S21) followed by a second irreversible process at even lower potentials. The first reduction is assigned to formation of the mixed-valent $\text{Fe}^{\text{II}}\text{Fe}^{\text{III}}$ species, but these are not stable since the cathodic peak and the anodic response in the reverse scan are separated by more than 600 mV at a scan rate of 100 mV/s. It is interesting to note, however, that

reduction of $\mathbf{1}^S$ ($E_p^{\text{red}} = -1.14$ V) seems to be more facile than reduction of $\mathbf{1}^O$ ($E_p^{\text{red}} = -1.32$), which is presumably due to a higher degree of electron delocalization in the thioether derivative. This observation is in accordance with the optical spectra, from which it was concluded that the *p*-OMe group in $\mathbf{1}^O$ transfers more electron density towards the $\{\text{Fe}_2\text{S}_2\}$ core than the *p*-SMe group in $\mathbf{1}^S$. Electrochemical measurements for $\mathbf{2}^C$, $\mathbf{2}^O$, and $\mathbf{2}^S$ under identical conditions revealed two sequential reduction processes with broadened anodic reverse peaks (**Table 2**, Figures S22 – S24). Again the thioether derivative $\mathbf{2}^S$ is easier to reduce than the ether analogue $\mathbf{2}^O$, and furthermore $\mathbf{2}^S$ has the lowest E_p^{red} (-0.99 V) of all complexes studied here.

DFT calculations. In order to corroborate the conclusions from structural and spectroscopic findings and to gain insight into the nature of the secondary bonding interactions in $\mathbf{2}^O$ and $\mathbf{2}^S$, DFT calculations were performed for complexes $\mathbf{1}^S$, $\mathbf{2}^O$, and $\mathbf{2}^S$. The pure BP86 functional (which for open-shell systems usually favors the low-spin state) has been used for both the antiferromagnetically coupled 1X as well as the ferromagnetically coupled 1X states, and the hybrid B3LYP functional (which usually predicts the high-spin state) has been tested for the ferromagnetically coupled state for comparison. In accordance with experimental findings, the BP86 results confirm that the singlet state is lower in energy (by 136, 110, and 66 kJ mol⁻¹ for $\mathbf{1}^S$, $\mathbf{2}^O$, and $\mathbf{2}^S$, respectively) than the high-spin state for all three models (Table 3). Calculated spin densities on the ether-O and thioether-S atoms are considered for evaluating the secondary interactions in $\mathbf{2}^O$ and $\mathbf{2}^S$, in comparison to $\mathbf{1}^S$ where no such interaction is present. The results collected in Table 3 show that there is no spin density on the pendent thioether groups for the $\mathbf{1}^S$ model, which confirms the expectation that there is no bonding interaction between those atoms. This is also validated by the atoms-in-molecules (AIM) analysis, which cannot detect any Fe–thioether bond in $\mathbf{1}^S$.

²⁰() Hoggins, J.T.; Steinfink, H. *Inorg. Chem.* **1976**, *15*, 1682-1685.

²¹() Gillum, W. O.; Frankel, R. B.; Foner, S.; Holm, R. H. *Inorg. Chem.* **1976**, *15*, 1095-1100.

²²() Beardwood, P.; Gibson, J. F. *Dalton Trans.* **1982**, 2015-2020.

²³() Wollenberg, M.; Berndt, C.; Bill, E.; Schwenn, J. D.; Seidler, A. *Eur. J. Biochem.* **2003**, *270*, 1662-1671.

²⁴() Simulation of the experimental magnetic data with a full-matrix diagonalization of exchange coupling and Zeeman splitting was performed with the julX program (E. Bill, Max-Planck Institute for Bioinorganic Chemistry, Mülheim/Ruhr, Germany). Before simulation the experimental data were corrected for the underlying diamagnetism by using tabulated Pascal constants (incremental method) and for temperature-independent paramagnetism (*TIP*). A Curie-Weiss-behaved paramagnetic impurity (*PI*) with spin $S = 5/2$ was included according to $\chi = (1 - PI) \cdot \chi + PI \cdot \chi_{\text{mono}}$. Best fit parameters for **1^C**: $J = -197 \text{ cm}^{-1}$, $PI = 1.7 \%$, $\chi(\text{TIP}) = 100 \cdot 10^{-6} \text{ cm}^3 \text{ mol}^{-1}$, $g = 2.000$ (fixed), $\theta_{\text{mono}} = -3.0 \text{ K}$ (fixed); for **1^O**: $J = -180 \text{ cm}^{-1}$, $PI = 0.5 \%$, $\chi(\text{TIP}) = 405 \cdot 10^{-6} \text{ cm}^3 \text{ mol}^{-1}$, $g = 2.000$ (fixed), $\theta_{\text{mono}} = -2.0 \text{ K}$ (fixed); for **1^S**: $J = -181 \text{ cm}^{-1}$, $PI = 0.8 \%$, $\chi(\text{TIP}) = 300 \cdot 10^{-6} \text{ cm}^3 \text{ mol}^{-1}$, $g = 1.898$ (fitted), $\theta_{\text{mono}} = -2.5 \text{ K}$ (fixed); for **2^C**: $J = -204 \text{ cm}^{-1}$, $PI = 1.6 \%$, $\chi(\text{TIP}) = 100 \cdot 10^{-6} \text{ cm}^3 \text{ mol}^{-1}$, $g = 2.000$ (fixed), $\theta_{\text{mono}} = -3.0 \text{ K}$ (fixed); for **2^O**: $J = -158 \text{ cm}^{-1}$, $PI = 2.3 \%$, $\chi(\text{TIP}) = 500 \cdot 10^{-6} \text{ cm}^3 \text{ mol}^{-1}$, $g = 1.855$ (fitted), $\theta_{\text{mono}} = -2.0 \text{ K}$ (fixed); for **2^S**: $J = -126 \text{ cm}^{-1}$, $PI = 5.8 \%$, $\chi(\text{TIP}) = 0 \text{ cm}^3 \text{ mol}^{-1}$, $g = 2.0$ (fixed), $\theta_{\text{mono}} = -1.0 \text{ K}$ (fixed).

²⁵() Ballmann, J.; Sun, X.; Dechert, S.; Bill, E.; Meyer, F. *J. Inorg. Biochem.* **2007**, *101*, 305-312.

²⁶() Palmer, G.; Dunham, W. R.; Fee, J. A.; Sands, R. H.; Iizuka, T.; Yonetani, T. *Biochim. Biophys. Acta* **1971**, *245*, 201-207.

Table 3: Relative energies, expectation values of the $\langle S^2 \rangle$ operator, and atomic spin densities ρ on the various atoms obtained at two different levels of theory (BP86/SVP or B3LYP/6-31G*) and with either antiferromagnetic (AF) or ferromagnetic (F) spin coupling.

complex	method	spin coupling	E_{rel} (kJ mol ⁻¹)	$\langle S^2 \rangle$	Spin densities ρ											
					Fe		^μ S (sulfide)		^L S (thiolate)				(thio)ether X			
1^S	BP86	AF	0.0	3.930	3.46	-3.46	-0.02	0.02	0.14	0.14	-0.14	-0.14	0.000	0.000	0.000	0.000
	BP86	F	+135.7	30.184	3.81	3.81	0.71	0.71	0.17	0.17	0.17	0.17	0.000	0.000	0.000	0.000
	B3LYP	F		30.042	3.74	3.74	0.78	0.78	0.20	0.19	0.20	0.19	0.004	0.004	0.004	0.004
2^O	BP86	AF	0.0	4.061	3.56	-3.56	-0.07	0.08	0.11	0.12	-0.13	-0.11	0.000	0.012		
	BP86	F	+109.6	30.016	3.84	3.84	0.73	0.72	0.15	0.16	0.15	0.15	0.000	0.014		
	B3LYP	F		30.039	3.76	3.76	0.80	0.79	0.18	0.19	0.18	0.18	0.009	0.015		
2^S	BP86	AF	0.0	4.171	3.59	-3.58	-0.06	0.05	0.11	0.10	-0.10	-0.11	0.035	-0.050		
	BP86	F	+66.5	30.019	3.81	3.81	0.72	0.72	0.13	0.15	0.14	0.13	0.061	0.046		
	B3LYP	F		30.042	3.74	3.73	0.79	0.80	0.17	0.17	0.17	0.17	0.062	0.0545		

On the other hand, for the 2^S model, significant spin density is found on the two thioether-S atoms (Figure 8), and non-negligible spin density is also found on the ether-O atoms of the 2^O model. While the spin density on the thioether-S atoms ($\sim 0.04 e$) is much lower than that on the thiolate ($0.10 e$) atoms, suggesting that the thioether bonds are weaker than the bonds to the other two groups, the density is still large enough to indicate a connection between the ferric ions and the thioether-S. This is also confirmed by the AIM analysis, which clearly detects a bond between the Fe ions and the thioether groups. The electronic density in the middle of these bonds (at the bond critical point) amounts to $0.03 e$ (Table S3 in ESI), which again is slightly lower than that of the Fe–sulfide and Fe–thiolate bonds (0.09 and $0.07 e$, respectively). For the 2^O model, the spin density on the ether-O atoms ($0.01 e$) is appreciably smaller than on the thioether atoms in the 2^S model, but still significant. Likewise, the AIM analysis identifies a bond between the Fe ions and the O atoms, with an electronic density ($0.02 e$) that is slightly lower than for the 2^S model. Thus, the calculations unambiguously confirm the existence of a Fe-thioether interaction in the 2^S model, albeit this is a relatively weak bond, and an even weaker bond in the 2^O model.

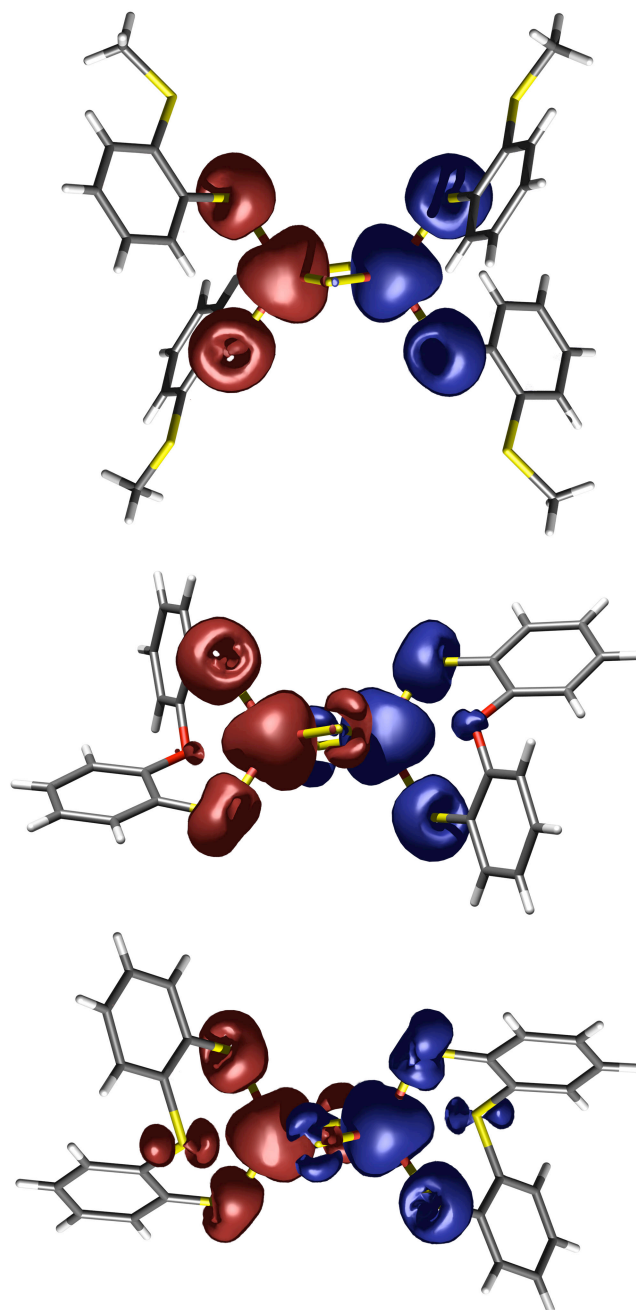


Figure 8. Spin densities (0.0035 a.u. level) for the 1^S (top), 2^O (middle), and 2^S (bottom) models, calculated at the BP86/def2-SVP level.

In order to rationalize the trend in the quadrupole splittings ΔE_Q observed in the Mössbauer spectra, eigenvalues of the electric field gradient (EFG) tensor have been calculated for the singlet states of the 1^S , 2^O , and 2^S models. Quadrupole splittings ΔE_Q derived from those values are compared with experimental data in Table 4. While the calculated values appear to be systematically too low by ~ 0.12 mm/s, the overall agreement with experimental values is quite

satisfying, and most importantly the trend for ΔE_Q ($1^S < 2^O < 2^S$) is almost quantitatively reproduced.

Table 4: Calculated eigenvalues of the field gradient tensor for the singlet states of 1^S , 2^O , and 2^S at the BP86/SVP level of theory, and calculated and experimental ΔE_Q values.

complex	calculated EFG ^a	ΔE_Q calculated [mm/s] ^b	ΔE_Q experimental [mm/s] ^c
1^S	0.169 / -0.0487 -0.120 (Fe1)	0.28	0.44
	0.168 / -0.0464 / -0.121 (Fe2)	0.28	
2^O	0.263 / -0.00184 / -0.261 (Fe1)	0.49	0.56
	0.266 / -0.0858 / -0.180 (Fe2)	0.44	
2^S	0.330 / -0.110 / -0.220 (Fe1)	0.54	0.61
	0.275 / -0.0765 / -0.199(Fe2)	0.46	

(a) the three eigenvalues of the field gradient tensor given in atomic units (1 a.u. = $9.72 \cdot 10^{21}$ V/m²). (b) ΔE_Q calculated according to $\Delta E_Q = \frac{1}{2}eQV_{zz} \cdot (1 + \eta^2/3)^{1/2}$, where the quadrupole moment Q is 0.16 barn ($0.16 \cdot 10^{-28}$ m²) for ⁵⁷Fe, V_{zz} is the main value of the EFG, $\eta = (V_{xx} - V_{yy})/V_{zz}$ (with $|V_{xx}| < |V_{yy}| < |V_{zz}|$), and 1 mm/s = $4.8075 \cdot 10^{-8}$ eV. (c) data from Table 2.

Conclusions

Secondary interactions between the ferric ions and added ether or thioether moieties do occur in oxidized [2Fe2S] clusters if the additional O or S donor atoms are suitably positioned in proximity to the cluster core. In the case of [2Fe2S] clusters with capping thiophenolate ligands this situation has to be enforced by a confined chelate arrangement, since no bonding interaction is observed when the tethered ether or thioether groups are free to rotate away from the metal. Due to the secondary interaction, which is clearly more pronounced for a thioether-S compared to an ether-O, the Fe atoms approach a trigonal bipyramidal coordination geometry with the additional donor atom and one of the bridging sulfides in apical positions. This gives rise to significant structural distortion of the cluster core with increasing Fe...Fe distances and widened Fe- μ S-Fe angles, which is reflected by marked changes in the spectroscopic and magnetic properties, in particular a distinct decrease in antiferromagnetic coupling and an increase in the Mössbauer quadrupole splitting. Considerable spin density is found on the fifth donor atom, and reduction is facilitated for the system with additional thioether-Fe bonds. Taken together, these

findings show that secondary bonding interactions can modulate the electronic properties of biological [2Fe2S] clusters, which may well play a role for, e.g., the unique [2Fe2S] cluster in biotin synthase with its unusual (and potentially chelating) arginine ligand. Indeed, the relevance of intermediates with five-coordinate Fe is known for some catalytic [4Fe4S] clusters.

Experimental Section

General Considerations. All manipulations were carried out under an anaerobic and anhydrous atmosphere of dry nitrogen by employing standard Schlenk techniques, or in a glove box. Et₂O was dried over sodium benzophenone ketyl, THF over potassium benzophenone ketyl, DMF, MeCN and DMSO-d₆ over CaH₂ and distilled prior to use. Glassware was dried at 120°C overnight. ¹H-NMR spectra were recorded on a Bruker Avance 500 MHz spectrometer at room temperature. Chemical shifts are reported in ppm relative to residual proton signals of DMSO-d₆ at 2.46 ppm. Microanalyses were performed by the "Analytisches Labor des Instituts für Anorganische Chemie der Universität Göttingen"; UV-Vis spectra were recorded with an Analytik Jena Specord S 100, using Schlenk quartz cuvettes. Mössbauer spectra were recorded on an alternating constant-acceleration spectrometer. Isomer shifts are given relative to iron metal at ambient temperature. Temperature-dependent magnetic susceptibilities of powdered samples were measured by using a SQUID magnetometer (MPMS-7, Quantum Design) at 1 T. 24 Cyclic voltammetry was performed with a potentiostat/galvanostat Perkin-Elmer Model 263A with glassy carbon working electrode and platinum reference and counter electrodes, in DMF/0.1 M [NBu₄]PF₆ at room temperature. Decamethylferrocene was used as internal standard. Compounds (NEt₄)₂[Fe₂S₂Cl₄],²⁷ 2-(methylthio)benzenethiol,²⁸ 2,2'-oxydibenzenethiol²⁹, 2,2'-thiodibenzenethiol³⁰ and 2,2'-methylenedibenzenethiol¹⁸ were synthesized according to reported methods. All other chemicals were used as purchased.

Bis(tetraethylammonium)-bis[di-(2-ethylthiophenolato)(μ-sulfido)ferrat(III)] (1^C). To a solution of 2-ethylbenzenethiol (1 g, tech. grade 90%, 6.5 mmol) in 20 ml THF at 0°C was added dropwise *n*-BuLi (4.1 ml, 1.6 M solution in hexane, 6.5 mmol) and the resulting yellow solution

was stirred at 0°C for 30 min. Then acetonitrile (10 ml), powdered (NEt₄)₂[Fe₂S₂Cl₄] (0.94 g, 1.63 mmol) and additional acetonitrile (20 ml) were added in this order. The reaction mixture was stirred for 20 min at 0°C and then for 1 h at room temperature. THF (40 ml) and Et₂O (40 ml) were added with agitation and the reaction mixture was left standing at -20°C for 2 d. The precipitate was filtered off, washed with Et₂O (20 ml) and dried in vacuum for 1 h. The obtained crude product was vigorously stirred in acetonitrile (30 ml) at room temperature for 3 h and insoluble byproducts were filtered off successively. The deep red filtrate was kept at -20°C for 4 d. The resulting black crystals were collected by filtration, washed with Et₂O and dried in vacuum over night to afford the pure product (500 mg, 0.51 mmol, 31%). ¹H-NMR (500 MHz, DMSO-d₆): δ = 1.09 (s_{br}, 24H, NEt₄), 1.29 (s_{br}, 12H, CH₃), 3.09 (s_{br}, 16H, NEt₄, 4H, Ar-H), 4.68 (s_{br}, 8H, CH₂), 9.18 (s_{br}, 4H, Ar-H), 10.19 (s_{br}, 4H, Ar-H). MS (ESI+) *m/z* (%): 1114 (100) [Fe₂S₂L₄(NEt₄)₃]⁺ (Figure S25). UV-Vis (DMF solution), λ_{max} [nm] (ε [M⁻¹cm⁻¹]): 331 (29000), 476 (15000). Elemental Analysis: Calcd.(%) for C₄₈H₇₆Fe₂N₂S₆: C 58.52, H 7.78, N 2.84, S 19.53. Found: C 57.97, H 7.75, N 2.83, S 19.07.

Bis(tetraethylammonium)-bis{di-[2-(methoxy)thiophenolato](μ-sulfido)ferrat(III)} (I⁰).

To a solution of 2-(methoxy)benzenethiol (1 ml, 1.15 g, 8.23 mmol) in 20 ml THF at 0°C was added dropwise *n*-BuLi (4.1 ml, 2.0 M solution in hexane, 8.23 mmol) and the reaction mixture was stirred for 1.5 h at room temperature. Then acetonitrile (20 ml), powdered (NEt₄)₂[Fe₂S₂Cl₄] (1.19 g, 2.05 mmol) and additional acetonitrile (20 ml) were added in this order. The resulting dark violet reaction mixture was stirred for 1 h. The precipitate, formed in the course of the reaction, was filtered off, washed with THF (20 ml) and Et₂O (20 ml) and dried in vacuum over night to afford a fine black powder (800 mg, 0.81mmol, 39%) of the product. Crystals were obtained by diffusion of Et₂O into deep violet solutions of the complex in DMF. ¹H-NMR (500 MHz, DMSO-d₆): δ = 1.13 (s_{br}, 24H, NEt₄), 3.12 (s_{br}, 16H, NEt₄, 4H, Ar-H), 3.88 (s_{br}, 12H, OMe), 9.00 (s_{br}, 4H, Ar-H), 10.19 (s_{br}, 4H, Ar-H). UV-Vis (DMF solution), λ_{max} [nm] (ε [M⁻¹cm⁻¹]):

1]): 296 (58000, *sh*), 336 (33000), 509 (15000). Elemental Analysis: Calcd.(%) for $C_{44}H_{68}Fe_2N_2O_4S_6$: C 53.21, H 6.90, N 2.82, S 18.96. Found: C 52.78, H 6.84, N 3.01, S 18.96.

Bis(tetraethylammonium)-bis{di-[2-(methylthio)thiophenolato](μ -sulfido)ferrat(III)} (1^S).

To a solution of 2-(methylthio)benzenethiol (1.27 g, 8.14 mmol) in 20 ml THF at 0°C was added dropwise *n*-BuLi (5.1 ml, 2.0 M solution in hexane, 8.14 mmol) and the resulting yellow solution was stirred at room temperature for 1.5 h. Acetonitrile (10 ml), $(NEt_4)_2[Fe_2S_2Cl_4]$ (1.18 g, 2.03 mmol) and an additional portion of acetonitrile (20 ml) were added to the reaction mixture. After stirring for 1 h the precipitate was filtered off, washed with a mixture of THF and MeCN (20 ml, v:v=1:1) and dried in vacuum. The crude product was dissolved in a minimum amount of DMF and layered with Et_2O (DMF: Et_2O =7:4, v:v). After completed diffusion, black crystals of the product (800 mg, 0.76 mmol, 37%) were separated by filtration and dried in vacuum. 1H -NMR (500 MHz, DMSO- d_6): δ = 1.13 (*s*_{br}, 24H, NEt_4), 2.37 (*s*_{br}, 12H, SMe), 3.12 (*s*_{br}, 16H, NEt_4), 3.29 (*s*_{br}, 4H, Ar-H), 9.18 (*s*_{br}, 4H, Ar-H), 10.06 (*s*_{br}, 4H, Ar-H). UV-Vis (DMF solution), λ_{max} [nm] (ϵ [$M^{-1}cm^{-1}$]): 307 (50000), 350 (27000, *sh*), 491 (12000). Elemental Analysis: Calcd.(%) for $C_{44}H_{68}Fe_2N_2S_{10}$: C 49.98, H 6.48, N 2.65. Found: C 49.68, H 6.63, N 2.62.

Bis(tetraethylammonium)-bis[(2,2'-methylenedibenzenethiolato)(μ -sulfido)ferrat(III)] (2^C). To a solution of 2,2'-methylenedibenzenethiol (720 mg, 3.10 mmol) in 20 ml THF at 0°C was added dropwise *n*-BuLi (3.90 ml, 1.6 M solution in hexanes, 6.20 mmol). After stirring for 30 min at 0°C, acetonitrile (10 ml), solid $(NEt_4)_2[Fe_2S_2Cl_4]$ (895 mg, 1.55 mmol) and further acetonitrile (20 ml) were added. The resulting reaction mixture was stirred for 20 min at 0°C and then 30 min at room temperature. The precipitate formed in the course of the reaction was filtered off and washed with THF (2×20 ml). The obtained brown solid was extracted with acetonitrile (6×40 ml). The combined extracts were condensed in to a volume of 120 ml and layered with Et_2O (120 ml). Diffusion at room temperature led to formation of small black crystals. Cooling the mixture to -20°C for 3 d completed the crystallization process. The product (490 mg, 0.55 mmol, 35%) was filtered off, washed with Et_2O (2×20 ml) and dried in vacuum. 1H -NMR (500 MHz, DMSO- d_6): δ = 1.14 (*s*_{br}, 24H, NEt_4), 2.68 (*s*_{br}, 4H, Ar-H), 3.12 (*s*_{br}, 16H,

NEt₄), 3.29 (s_{br}, 4H, CH₂), 5.44 (s_{br}, 4H, Ar-H), 8.98 (s_{br}, 4H, Ar-H), 9.63 (s_{br}, 4H, Ar-H). MS (ESI+) *m/z* (%): 1026 (100) [Fe₂S₂L₂(NEt₄)₃]⁺ (Figure S26). UV-Vis (DMF solution), λ_{max} [nm] (ε [M⁻¹cm⁻¹]): 291 (16000), 352 (20500), 444(10000), 547 (10500), 616 (6500). HiRes-MS (ESI+): Calcd.(*m/z*) for C₅₀H₈₀Fe₂N₃S₆: 1026.33723. Found: 1026.33675 (Figure S27).

Bis(tetraethylammonium)-bis[(2,2'-oxydibenzenethiolato)(μ-sulfido)ferrat(III)] (2^O). To a solution of 2,2'-oxydibenzenethiol (1.38 g, 5.88 mmol) in 30 ml THF at 0°C was added dropwise *n*-BuLi (5.9 ml, 2.0 M solution in hexane, 11.80 mmol). After stirring for 20 min at 0°C, acetonitrile (15 ml), solid (NEt₄)₂[Fe₂S₂Cl₄] (1.7 g, 2.95 mmol) and additional acetonitrile (35 ml) were added. The resulting dark reaction mixture was allowed to warm to room temperature over night. The precipitate was separated by filtration, washed with acetonitrile (2×20 ml) and dried in vacuum for 2 h. The crude product was dissolved in DMF (200 ml), Et₂O (160 ml) was added and the solution was left standing at -20°C for 2 d. Crystallization was completed by addition of further Et₂O (80 ml). After 1 d at -20°C black crystals of the product (800 mg, 0.89 mmol, 30%) were filtered off, washed with Et₂O (2×20 ml) and dried in vacuum. ¹H-NMR (500 MHz, DMSO-d₆): δ = 1.15 (s_{br}, 24H, NEt₄), 3.15 (s_{br}, 16H, NEt₄), 3.59 (s_{br}, 4H, Ar-H), 5.76 (s_{br}, 4H, Ar-H), 8.41 (s_{br}, 4H, Ar-H), 9.60 (s_{br}, 4H, Ar-H). UV-Vis (DMF solution), λ_{max} [nm] (ε [M⁻¹cm⁻¹]): 329 (19000), 486 (9000). Elemental Analysis: Calcd.(%) for C₄₀H₅₆Fe₂N₂O₂S₆: C 53.32, H 6.26, N 3.11, S 21.35. Found: C 52.13, H 6.21, N 3.46, S 20.70.

Bis(tetraethylammonium)-bis[(2,2'-thiodibenzenethiolato)(μ-sulfido)ferrat(III)] (2^S). To a solution of 2,2'-thiodibenzenethiol (900 mg, 3.60 mmol) in 20 ml THF at 0°C was added dropwise *n*-BuLi (3.6 ml, 2.0 M solution in hexane, 7.20 mmol). After stirring for 20 min at 0°C, acetonitrile (10 ml) was added and the reaction mixture cooled to -20°C. Then powdered (NEt₄)₂[Fe₂S₂Cl₄] (1.04 g, 1.80 mmol) and additional acetonitrile (20 ml) were added. The resulting dark reaction mixture was slowly allowed to warm to room temperature over a period of 4 h. The black precipitate formed was separated by filtration, washed with acetonitrile (2×20 ml) and dried in vacuum for 1 h. The crude product was extracted with DMF (5×20 ml)

yielding a deep purple solution, and Et₂O (80 ml) was added with agitation. The mixture was left standing at room temperature for 3 h causing initial crystal formation. After 4 d at -20°C crystallization was completed. The precipitate was filtered off, washed with Et₂O (30 ml) and dried in vacuum to afford black crystals of the product (250 mg, 0.27 mmol, 15%). ¹H-NMR (500 MHz, DMSO-d₆): δ = 1.15 (s_{br}, 24H, NEt₄), 3.10 (s_{br}, 16H, NEt₄), 3.57 (s_{br}, 4H, Ar-H), 9.00 (s_{br}, 4H, Ar-H), 9.13 (s_{br}, 4H, Ar-H), 10.29 (s_{br}, 4H, Ar-H). UV-Vis (DMF solution), λ_{max} [nm] (ε [M⁻¹cm⁻¹]): 288 (59000), 322 (37000, *sh*), 475 (11000). Elemental Analysis: Calcd.(%) for C₄₀H₅₆Fe₂N₂S₈: C 51.49, H 6.05, N 3.00. Found: C 50.50, H 6.42, N 3.34.

Computations. DFT calculations were performed with the Turbomole 5.9 software³¹ using the Becke–Perdew-1986 functional (BP86)³² and the def2-SVP basis set³³. Electric field gradients were calculated with the same method. Atoms-in-molecules (AIM) analysis³⁴ was performed with the Gaussian-03 software³⁵, with the B3LYP method³⁶ and the DZpdf basis set for Fe³⁷ and the 6-31G* basis set for all the other atoms³⁸. For technical reasons, the latter calculations were performed only for the ferromagnetically coupled state.

X-ray Crystallography. The crystal data and details of the data collections are given in Table 3. X-ray data were collected on a STOE IPDS II diffractometer (graphite monochromated Mo-Kα radiation, λ = 0.71073 Å) by use of ω scans at -140 °C. The structures were solved by direct methods and refined on *F*² using all reflections with SHELX-97.³⁹ Atoms of the disordered parts of **1**^C were refined isotropically, all other non-hydrogen atoms were refined anisotropically. Hydrogen atoms were placed in calculated positions and assigned to an isotropic displacement parameter of 0.08 Å². Crystals of **2**^S are non-merohedrally twinned (ratio of the two twin components approximately 70 : 30, twinlaw 1, 0, 0 / 0, -1, 0 / -0.35, 0, -1) and the reflection data for refinement were prepared using the program X-AREA.⁴⁰ The absolute structure parameter of **2**^S (*x* = -0.01(4)) was determined according to Flack⁴¹ with SHELX-97. The ethyl groups of **1**^C

and the acetonitrile solvent molecule were found to be disordered about two positions ((occupancy factors of 0.562(16)/0.438(16) (C8), 0.681(16)/0.319(16) (C16), and 0.64(3)/0.36(3) (N3, C33, C34)). Additionally two NEt_4^+ cations in $\mathbf{1}^{\text{C}}$ are disordered about special positions and were refined with fixed occupancy factors of 0.5. DFIX restraints (Ph-Et: $d_{\text{C-C}} = 1.51 \text{ \AA}$; MeCN: $d_{\text{C-C}} = 1.47 \text{ \AA}$, $d_{\text{C=N}} = 1.14 \text{ \AA}$; NEt_4^+ : $d_{\text{C-N}} = 1.51 \text{ \AA}$) and EADP constraints (C16A/B) were used to model the disorder. Face-indexed absorption corrections for $\mathbf{1}^{\text{C}}$, $\mathbf{1}^{\text{O}}$, $\mathbf{1}^{\text{S}}$, $\mathbf{2}^{\text{C}}$, and $\mathbf{2}^{\text{O}}$ were performed numerically with the program X-RED.⁴²

²⁷() Do, Y.; Simhon, E. D.; Holm, R. H. *Inorg. Chem.* **1983**, *22*, 3809-3812.

²⁸() Sellmann, D.; Schillinger, H.; Knoch, F. *Z. Naturforsch. B* **1992**, *47*(5), 748-753.

²⁹() Alvarado-Rodríguez, J. G.; Andrade-López, N.; Gonzáles-Montiel, S.; Merino, G.; Vela, A. *Eur. J. Inorg. Chem.* **2003**, *19*, 3554-3562.

³⁰() Sellmann, D.; Häußinger, D.; Heinemann, F. W. *Eur. J. Inorg. Chem.* **1999**, *10*, 1715-1725.

³¹() Ahlrichs, R.; Bär, M.; Häser, M.; Horn, H.; Kölmel, C. *Chem. Phys. Lett.* **1989**, *162*, 165-169.

³²() (a) Becke, A. D. *Phys. Rev. A* **1988**, *38*, 3098-3100. (b) Perdew, J. P. *Phys. Rev. B* **1986**, *33*, 8822-8824.

³³() Weigend, F.; Ahlrichs, R. *Phys. Chem. Chem. Phys.* **2005**, *7*(18), 3297-3305.

³⁴() (a) Bader, R. F. W. *Atoms in Molecules: A Quantum Theory*, Oxford University Press, Oxford **1990**. Cioslowski, J. *Chem. Phys. Lett.* **1992**, *194*, 73-78.

³⁵() Gaussian 03, Revision C.02, Frisch, M. J.; Trucks, G. W.; Schlegel, H. B.; Scuseria, G. E.; Robb, M. A.; Cheeseman, J. R.; Montgomery, Jr., J. A.; Vreven, T.; Kudin, K. N.; Burant, J. C.; Millam, J. M.; Iyengar, S. S.; Tomasi, J.; Barone, V.; Mennucci, B.; Cossi, M.; Scalmani, G.; Rega, N.; Petersson, G. A.; Nakatsuji, H.; Hada, M.; Ehara, M.; Toyota, K.; Fukuda, R.; Hasegawa, J.; Ishida, M.; Nakajima, T.; Honda, Y.; Kitao, O.; Nakai, H.; Klene, M.; Li, X.; Knox, J. E.; Hratchian, H. P.; Cross, J. B.; Bakken, V.; Adamo, C.; Jaramillo, J.; Gomperts, R.; Stratmann, R. E.; Yazyev, O.; Austin, A. J.; Cammi, R.; Pomelli, C.; Ochterski, J. W.; Ayala, P. Y.; Morokuma, K.; Voth, G. A.; Salvador, P.; Dannenberg, J. J.; Zakrzewski, V. G.; Dapprich, S.; Daniels, A. D.; Strain, M. C.; Farkas, O.; Malick, D. K.; Rabuck, A. D.; Raghavachari, K.; Foresman, J. B.; Ortiz, J. V.; Cui, Q.; Baboul, A. G.; Clifford, S.; Cioslowski, J.; Stefanov, B. B.; Liu, G.; Liashenko, A.; Piskorz, P.; Komaromi, I.; Martin, R. L.; Fox, D. J.; Keith, T.; Al-Laham, M. A.; Peng, C. Y.; Nanayakkara, A.; Challacombe, M.; Gill, P. M. W.; Johnson, B.; Chen, W.; Wong, M. W.; Gonzalez, C.; Pople, J. A. *Gaussian, Inc.*, Wallingford CT **2004**.

³⁶() (a) Becke, A. D. *J. Chem. Phys.* **1993**, *98*, 5648-5652. (b) Stephens, P. J.; Devlin, F. J.; Frisch, M. J.; Chabalowski, C. F. *J. Phys. Chem.* **1994**, *98*, 11623-11627.

³⁷() Sigfridsson, E.; Ryde, U. *J. Biol. Inorg. Chem.* **1999**, *4*, 99-110.

³⁸() Hehre, W. J.; Radom, L.; Schleyer, P. v. R.; Pople, J. A. *In Ab initio molecular orbital theory*, Wiley-Interscience, New York **1986**.

³⁹() (a) Sheldrick, G. M. *SHELXL-97, Program for Crystal Structure Refinement*; University of Göttingen: Göttingen, Germany, 1997. (b) Sheldrick, G. M. *SHELXS-97, Program for Crystal Structure Solution*; University of Göttingen: Göttingen, Germany, 1997.

⁴⁰() *X-AREA*; STOE & CIE GmbH: Darmstadt, Germany, 2002.

⁴¹() Flack, H. D. *Acta Crystallogr.* **1983**, *A39*, 876-881.

⁴²() *X-RED*; STOE & CIE GmbH: Darmstadt, Germany, 2002.

Table 4: Crystal data and refinement details for all new complexes.

	1 ^c	1 ^o	1 ^s	2 ^c	2 ^o	2 ^s
empirical formula	[C ₃₂ H ₃₆ Fe ₂ S ₆] ²⁻ , 2 (C ₈ H ₂₀ N ⁺), 2 MeCN	[C ₂₈ H ₂₈ Fe ₂ O ₄ S ₆] ²⁻ , 2 (C ₈ H ₂₀ N ⁺)	[C ₂₈ H ₂₈ Fe ₂ S ₁₀] ²⁻ , 2 (C ₈ H ₂₀ N ⁺)	[C ₂₆ H ₂₀ Fe ₂ S ₆] ²⁻ , 2 (C ₈ H ₂₀ N ⁺)	[C ₂₄ H ₁₆ Fe ₂ O ₂ S ₆] ²⁻ , 2 (C ₈ H ₂₀ N ⁺)	[C ₂₄ H ₁₆ Fe ₂ S ₈] ²⁻ , 2 (C ₈ H ₂₀ N ⁺)
formula weight	1067.28	993.06	1057.30	896.98	900.93	933.05
crystal size [mm]	0.50 × 0.47 × 0.45	0.46 × 0.38 × 0.15	0.43 × 0.37 × 0.25	0.38 × 0.32 × 0.26	0.40 × 0.36 × 0.32	0.32 × 0.07 × 0.06
crystal system	monoclinic	monoclinic	monoclinic	monoclinic	monoclinic	monoclinic
space group	<i>C2/c</i> (No. 15)	<i>P2₁/c</i> (No. 14)	<i>P2₁/n</i> (No. 14)	<i>P2₁/n</i> (No. 14)	<i>P2₁/c</i> (No. 14)	<i>P2₁</i> (No. 14)
<i>a</i> [Å]	17.7778(8)	9.9311(4)	10.7835(4)	11.4189(6)	16.1247(6)	9.4152(7)
<i>b</i> [Å]	14.5054(5)	21.7363(7)	17.5216(6)	11.5647(4)	13.3743(4)	13.1074(11)
<i>c</i> [Å]	22.5604(11)	22.5717(10)	14.4262(6)	16.5968(9)	19.7471(7)	17.7976(16)
β [°]	97.015(4)	94.367(3)	109.692(3)	95.162(4)	90.234(3)	95.289(6)
<i>V</i> [Å ³]	5774.2(4)	4858.3(3)	2566.34(17)	2182.82(18)	4258.6(3)	2187.0(3)
$\rho_{\text{calcd.}}$ [g cm ⁻³]	1.228	1.358	1.368	1.365	1.405	1.417
<i>Z</i>	4	4	2	2	4	2
<i>F</i> (000)	2280	2104	1116	948	1896	980
μ [mm ⁻¹]	0.755	0.897	1.004	0.983	1.012	1.076
<i>T</i> _{max} / <i>T</i> _{min}	0.7364 / 0.6709	0.8490 / 0.6252	0.8188 / 0.6693	0.8154 / 0.6726	0.7843 / 0.6765	-
<i>hkl</i> range	±20, ±17, ±26	-11 - 10, ±25, ±26	-13 - 12, ±21, ±17	-12 - 13, ±13, ±19	±20, ±17, ±25	-10 - 11, ±15, -21 - 20
θ range [°]	1.82 - 24.81	1.30 - 24.85	1.90 - 25.90	2.08 - 24.78	1.84 - 27.38	2.17 - 24.85
measured refl.	41296	67941	43925	29971	82478	10276
unique refl. [<i>R</i> _{int}]	4967 [0.0297]	8378 [0.0660]	4969 [0.0500]	3750 [0.0449]	9602 [0.0446]	4981 [0.1106]
observed refl. <i>I</i> > 2 σ (<i>I</i>)	4604	6504	4464	3336	7608	3047
ref. param / constr.	292 / 24	535 / 0	268 / 0	239 / 0	477 / 0	477 / 1
goodness-of-fit	1.119	1.017	1.043	1.039	1.038	1.006
<i>R</i> 1, <i>wR</i> 2 (<i>I</i> > 2 σ (<i>I</i>))	0.0800, 0.1919	0.0273, 0.0588	0.0247, 0.0653	0.0227, 0.0595	0.0279, 0.0654	0.0598, 0.0976
<i>R</i> 1, <i>wR</i> 2 (all data)	0.0837, 0.1934	0.0416, 0.0610	0.0289, 0.0667	0.0269, 0.0606	0.0410, 0.0683	0.1064, 0.1085
resid. el. dens. [e Å ⁻³]	1.057 / -0.650	0.314 / -0.214	0.300 / -0.197	0.294 / -0.206	0.329 / -0.272	0.457 / -0.330

Acknowledgment. We sincerely thank Jörg Teichgräber for collecting the CV data. Financial support by the DFG (International Research Training Group GRK 1422 "Metal Sites in Biomolecules: Structures, Regulation and Mechanisms") and the Fonds der Chemischen Industrie (Kekulé fellowship for J.B.) is gratefully acknowledged.

Supporting Information Available: